

Cold neutron scattering in imperfect deuterium crystals

Andrzej Adamczak*

*Institute of Nuclear Physics, Polish Academy of Sciences,
Radzikowskiego 152, PL-31342 Kraków, Poland*

(Dated: June 5, 2022)

Abstract

The differential cross sections for cold neutron scattering in mosaic deuterium crystals have been calculated for various target temperatures. The theoretical results are compared with the recent experimental data for the neutron wavelengths $\lambda \approx 1\text{--}9 \text{ \AA}$. It is shown that the structures of observed Bragg peaks can be explained by the mosaic spread of about 3° and contributions from a limited number of crystal orientations. Such a crystal structure should be also taken into account in ultracold neutron upscattering due to the coherent phonon annihilation in solid deuterium.

PACS numbers: 28.20.Cz, 67.80.F-

*Electronic address: andrzej.adamczak@ifj.edu.pl

I. INTRODUCTION

The aim of this work is a calculation of the differential cross sections for cold neutron scattering in solid molecular deuterium (sD_2) at various temperatures and comparison with the recent experimental data [1, 2]. Deceleration of cold neutrons in sD_2 converters is an effective method for production of high-intensity ultracold neutron sources [1–9]. Therefore knowledge of the neutron cross sections is indispensable for effective projecting such sources. Ultracold neutrons (UCN) are applied for studies of fundamental properties of the neutron [10, 11]. Also, they can be used for surface physics [12], investigations of the neutron mirror-neutron oscillations [13] and neutron quantum states in the gravitational potential [14].

The experimental total cross sections [1, 2] in the Bragg-scattering region display a certain number of pronounced peaks. Their heights decrease when sD_2 temperature is rising from 8 K to 18 K. However, for a fixed crystal, the structure of Bragg peaks does not practically change with varying temperature. It is well known that sD_2 at such temperatures and under low pressure has the hcp structure [15, 16], which has been confirmed using the Raman spectroscopy [7]. A simple calculation of the Bragg cross sections presented in Ref. [1] does not lead to agreement with the experiment, both for the random polycrystalline hcp structure and for a few specifically oriented hcp polycrystals. The magnitudes of the theoretical peaks are too large. Also, these peaks are sharp, while the experimental peaks are quite broad. Moreover, the observed and calculated locations of the Bragg peaks do not fully coincide. A more advanced calculation of the total cross section for a random polycrystalline sD_2 [17], with incoherent processes taken into account, also disagrees with the experiment in the Bragg-scattering region.

A calculation of the cross sections presented in this paper includes both the elastic and inelastic processes in the sD_2 lattice and in D_2 molecules. Rotational and vibrational transitions in these molecules, which are due to collisions with neutrons, are taken into account. Interactions of neutrons with phonons are described in the incoherent approximation while the incoherent and coherent elastic cross sections are treated separately. The coherent elastic scattering of neutrons is considered both for the random polycrystalline hcp structure and for different orientations of the hcp monocrystal.

The calculated total cross sections are compared with the available data for the neutron wavelengths $\lambda \approx 1\text{--}9 \text{ \AA}$ [1, 2], with the experimental uncertainty of neutron wavelength taken into account. Since this uncertainty is much smaller than the observed widths of the Bragg peaks [18], an explanation of this effect by the presence of mosaic imperfections in the sD_2 crystals is studied. Most crystals are perfect only in very small domains (mosaic blocks) on the order of 1000 \AA , which are separated by displacements and distortions in the lattice. These domains are almost parallel, with small deviations of their orientations from the main direction. Such angular deviations are usually well-described by a Gaussian distribution [19]. The mosaic spread may reach even a few degrees in certain crystals.

Another experimental problem is connected with different structures of the sD_2 crystals, which are grown even in very similar conditions. As a result, the experimental Bragg cross sections for the sD_2 crystals, obtained by freezing D_2 gas and two samples of liquid D_2 , are different [1, 2]. In this paper, such a phenomenon is ascribed to different orientations of large monocrystals (much greater than the mosaic blocs) that are present in a given sD_2 target. These orientations differ much greater than those of microscopic mosaic blocs within a single monocrystal. Such a model of a real deuterium target is suggested by the optical observations of growing sD_2 [1, 7].

II. METHOD OF CALCULATION

Interaction of the neutron with a single deuterium nucleus is described using the Fermi pseudopotential [20]. The partial differential cross section for neutron scattering in sD_2 can be expressed in terms of the Van Hove response function \mathcal{S} [21], which depends on the target properties for fixed momentum transfer and energy transfers. When the impinging neutron causes a rotational-vibrational transition in a deuterium molecule bound in the sD_2 lattice, the corresponding cross section can be expressed as follows

$$\left(\frac{\partial^2 \sigma}{\partial \Omega \partial \varepsilon'} \right)_{0n} = \frac{k'}{k} \sigma_{0n} \mathcal{S}_i(\boldsymbol{\kappa}, \omega), \quad (1)$$

where \mathcal{S}_i denotes the incoherent response function, which is a fraction of the total response function \mathcal{S} [22]. The energy transfer ω and the momentum transfer $\boldsymbol{\kappa}$ to the sD_2 lattice are defined as (in the atomic units)

$$\omega = \varepsilon - \varepsilon' - \Delta E, \quad \boldsymbol{\kappa} = \mathbf{k} - \mathbf{k}', \quad (2)$$

where ε and ε' stand for the initial and final kinetic energies of the neutron and ΔE is the internal-energy change of the target molecule due to the rotational-vibrational transition. Vectors \mathbf{k} and \mathbf{k}' denote the initial and final neutron momenta, respectively. The usual relations between the kinetic energies ε and ε' and the corresponding absolute values k and k' of neutron momenta are fulfilled

$$\varepsilon = k^2/2m_n, \quad \varepsilon' = k'^2/2m_n, \quad (3)$$

m_n being the neutron mass. Function σ_{0n} in Eq. (1) is the squared modulus of neutron scattering amplitude for a single bound molecule

$$\sigma_{0n} = |\mathcal{F}_{0n}|^2, \quad (4)$$

averaged over the total spin of the neutron and D_2 system. The indices $(0) = (0K)$ and $(n) = (\nu K')$ denote the initial and final rotational-vibrational states, respectively. In the case of considered target temperatures, all the molecules are initially in the ground vibrational state. The final vibrational state is characterized by the quantum number ν . The quantum numbers K and K' correspond to the initial and final rotational states of D_2 .

When $\Delta E = 0$, for all the molecules in sD_2 , neutron scattering may be strictly elastic (no simultaneous phonon processes) or quasielastic (with phonon creation or annihilation). It is conventional to separately calculate the coherent and incoherent fractions of the corresponding differential cross section. The coherent cross section, which displays strong interference effects from all lattice sites, takes the general form [22]

$$\left(\frac{\partial^2 \sigma}{\partial \Omega \partial \varepsilon'} \right)_{\text{coh}} = \frac{k'}{k} \sigma_{\text{coh}} \mathcal{S}(\boldsymbol{\kappa}, \omega), \quad (5)$$

per one D_2 molecule. The coherent elastic cross section σ_{coh} for a single bound molecule is defined as

$$\sigma_{\text{coh}} = |\overline{\mathcal{F}_{00}}|^2. \quad (6)$$

The horizontal bar denotes here averaging over a random distribution of the total spin of the $n + D_2$ system and over the molecular rotational population in the lattice. The value I of total spin of the symmetric molecule D_2 is equal to $I = 0, 2$ for even rotational numbers K (ortho- D_2) and $I = 1$

for odd rotational numbers (para-D₂). In solid deuterium, the two rotational states $K = 0$ and $K = 1$ are usually present, since the rotational relaxation $K = 1 \rightarrow K' = 0$ is very slow without a catalyst [16]. It is assumed that there is no correlation between the spin \mathbf{I} and the location of D₂ in the sD₂ lattice.

The incoherent cross section for neutron scattering in sD₂ ($\Delta E = 0$) is expressed by the formula similar to Eq. (1) [22]

$$\left(\frac{\partial^2 \sigma}{\partial \Omega \partial \varepsilon'} \right)_{\text{inc}} = \frac{k'}{k} \sigma_{\text{inc}} \mathcal{S}_i(\mathbf{\kappa}, \omega), \quad (7)$$

where σ_{inc} is the incoherent elastic cross section for neutron scattering from a single bound molecule

$$\sigma_{\text{inc}} = \overline{|\mathcal{F}_{00}|^2} - |\overline{\mathcal{F}_{00}}|^2 = \overline{|\mathcal{F}_{00}|^2} - \sigma_{\text{coh}}. \quad (8)$$

The functions σ_{0n} , σ_{coh} , and σ_{inc} have been calculated similarly as the analogous quantities for the muonic atom scattering in gaseous and solid hydrogenic targets [23, 24]. Since the muonic atoms are small neutral objects, the methods of evaluation of the cross sections for these atoms are almost the same as for neutrons. Therefore, it is sufficient to use the neutron mass, scattering lengths, and appropriate spin correlations [25, 26] in the general equations from Refs. [23, 24]. As a result, in the case of $n + \text{D}_2$ scattering one obtains

$$\sigma_{0n} = \begin{cases} (4b_{\text{coh}}^2 + \frac{5}{2}b_{\text{inc}}^2) f_{KK'}(\kappa) & \text{even } K \text{ and } K', \\ \frac{3}{2} b_{\text{inc}}^2 f_{KK'}(\kappa) & \text{even } K, \text{ odd } K', \\ 3b_{\text{inc}}^2 f_{KK'}(\kappa) & \text{odd } K, \text{ even } K', \\ (4b_{\text{coh}}^2 + b_{\text{inc}}^2) f_{KK'}(\kappa) & \text{odd } K \text{ and } K', \end{cases} \quad (9)$$

where $b_{\text{coh}} = 6.671$ fm and $b_{\text{inc}} = 4.04$ fm denote, respectively, the coherent and incoherent scattering length for neutron scattering from a bound deuterium nucleus. The molecular form factor $f_{KK'}$ is defined as

$$f_{KK'}(\kappa) = \sum_l \mathcal{W}_{K'lK} |\mathcal{D}_{\nu l}(\kappa)|^2, \quad (10)$$

with the angular-momentum factor $\mathcal{W}_{K'lK}$

$$\mathcal{W}_{K'lK} \equiv (2K' + 1)(2l + 1) \begin{pmatrix} K' & l & K \\ 0 & 0 & 0 \end{pmatrix}^2, \quad \mathcal{W}_{K0K} = 1 \quad (11)$$

expressed by the Wigner $3j$ symbols. Equation (11) has been obtained upon averaging σ_{0n} over projections of the initial angular momentum of D₂ and summing over projections of the final angular momentum of this molecule. Function $\mathcal{D}_{\nu l}$ in Eq. (10) denotes the radial matrix element

$$\begin{aligned} \mathcal{D}_{\nu l}(\kappa) &\equiv \int_0^\infty dR \chi_\nu(R) j_l(\kappa R/2) \chi_0(R), \\ \mathcal{D}_{\nu l}(\kappa) &\xrightarrow{\kappa \rightarrow 0} \begin{cases} 1 & \text{when } \nu = 0 \text{ and } l = 0, \\ 0 & \text{otherwise,} \end{cases} \end{aligned} \quad (12)$$

in which j_l is the l th spherical Bessel function. The radial wave function of the D₂ molecule for the vibrational state ν is denoted here by χ_ν and R stands for the internuclear distance in D₂. Numerical evaluation of the matrix elements (12) has been performed assuming that the vibrations

of D_2 are harmonic and that there is no coupling between the molecular vibrations and rotations. Employing the harmonic-potential model of D_2 instead of the rigid-rotor model leads to accurate cross sections even at high collision energies.

The coherent elastic cross section (6) is expressed by the coherent scattering length b_{coh} and the radial matrix element (12) for $\nu = 0$ and $l = 0$

$$\sigma_{\text{coh}} = \begin{cases} 4b_{\text{coh}}^2 |\mathcal{D}_{00}(\kappa)|^2 & \text{for } K = K', \\ 0 & \text{otherwise.} \end{cases} \quad (13)$$

In the case of harmonic hcp lattice, the incoherent response function \mathcal{S}_i in Eqs. (1) and (7) is approximated by the phonon expansion of \mathcal{S}_i for a Bravais cubic lattice [22, 27]

$$\mathcal{S}_i(\kappa, \omega) = \exp(-2W) \left[\delta(\omega) + \sum_{n=1}^{\infty} g_n(\omega) \frac{(2W)^n}{n!} \right], \quad (14)$$

in which $\exp(-2W) = \exp[-2W(\kappa)]$ denotes the Debye-Waller factor. The functions g_n are defined as

$$\begin{aligned} g_1(\omega) &= \frac{1}{2W} \frac{\kappa^2}{2M_{\text{mol}}} \frac{Z(\omega)}{\omega} [n_B(\omega) + 1], \\ g_n(\omega) &= \int_{-\infty}^{\infty} d\omega' g_1(\omega - \omega') g_{n-1}(\omega'), \\ \int_{-\infty}^{\infty} d\omega g_n(\omega) &= 1, \end{aligned} \quad (15)$$

where M_{mol} is the mass of D_2 molecule, $Z(\omega)$ is the normalized density of vibrational states of the lattice, and n_B denotes the Bose phonon-population factor

$$n_B(\omega) = [\exp(\omega/k_B T) - 1]^{-1}, \quad (16)$$

for a given temperature T (k_B is the Boltzmann constant). The first term in the phonon expansion (14) corresponds to recoil-less scattering from a rigid sD_2 lattice. When $\Delta E = 0$, such a scattering cannot change the neutron kinetic energy because of a very large mass of the sD_2 target. The next terms describe neutron scattering and possible rotational-vibrational transitions in D_2 with simultaneous creation ($\omega > 0$) or annihilation ($\omega < 0$) of phonons. In particular, the second term in Eq. (14) is connected with one-phonon processes. Equations (15) have been derived assuming that $Z(-\omega) \equiv Z(\omega)$.

Evaluation of the incoherent cross section has been performed using the isotropic Debye model, characterized by the following density of vibrational states

$$Z(\omega) = \begin{cases} 3\omega^2/\omega_D^3 & \text{if } \omega \leq \omega_D \\ 0 & \text{if } \omega > \omega_D, \end{cases} \quad (17)$$

where $\omega_D = k_B \Theta_D$ denotes the Debye energy corresponding to the Debye temperature Θ_D . In the case of solid hydrogenic targets at low pressures, Θ_D equals about 100 K and it slowly decreases with rising target temperature [15]. For the calculation of cross sections at various temperatures, the following estimation of the Debye temperature

$$\Theta_D = 2^{1/2} (3\pi^2)^{1/3} \beta \frac{c_s}{a_{\text{hcp}} k_B}, \quad (18)$$

has been used. The sound velocity c_s and the molar volume of sD₂ for calculation of the lattice constant a_{hcp} have been taken from Ref. [16]. A constant correction factor $\beta = 1.085$ in Eq. (18) is introduced to fit the experimental value of 114 K for sD₂ at zero temperature [28]. As a result, one obtains $\Theta_D = 110$ K for 8-K sD₂ and $\Theta_D = 104$ K for 18-K sD₂.

The exponent $2W$ of the Debye-Waller factor for a cubic lattice takes the form [22]

$$2W = \frac{1}{3} \langle \mathbf{u}^2 \rangle \kappa^2, \quad (19)$$

where $\langle \mathbf{u}^2 \rangle$ is the mean square displacement of the molecule from its lattice site. In the case of harmonic crystal, Eq. (19) can be estimated using the expression

$$2W = \frac{\kappa^2}{2M_{\text{mol}}} \int_0^\infty d\omega \coth\left(\frac{\omega}{2k_B T}\right) \frac{Z(\omega)}{\omega}. \quad (20)$$

This expression is employed here as a good approximation for a harmonic hcp lattice. For a 5-K sD₂ crystal, Eqs. (18) and (20) lead to the root-mean-square displacement of 0.50 Å, which is in excellent agreement with the experimental result from Ref. [28].

The calculation of all phonon cross sections is performed here in the incoherent approach, which is achieved by substituting $\sigma_{\text{inc}} + \sigma_{\text{coh}}$ for σ_{inc} in the nonelastic fraction of Eq. (7). As a result, only the elastic Bragg scattering is taken into account in the coherent cross section (5). This is a very good approach at $\varepsilon \gtrsim 1$ meV. For a perfect lattice, the coherent elastic cross section per one molecule has the form of a sum over the reciprocal-lattice vectors $\boldsymbol{\tau}$ [22]

$$\left(\frac{d\sigma}{d\Omega}\right)_{\text{coh}}^{\text{el}} = \frac{(2\pi)^3}{V_0} \sum_{\boldsymbol{\tau}} |F_N(\boldsymbol{\tau})|^2 \delta(\boldsymbol{\kappa} - \boldsymbol{\tau}) \exp(-2W), \quad (21)$$

where V_0 denotes the unit-cell volume and $|F_N(\boldsymbol{\tau})|^2$ is the average squared unit-cell factor

$$|F_N(\boldsymbol{\tau})|^2 = \sigma_{\text{coh}} \frac{1}{N} \left| \sum_{d=1}^N \exp(i\boldsymbol{\tau} \cdot \mathbf{d}) \right|^2. \quad (22)$$

Vector \mathbf{d} denotes here the position of a given molecule in the unit cell and N is the number of molecules per unit cell. The unit cell of hcp sD₂ lattice contains two molecules. From Eq. (21) it follows that the Bragg scattering takes place only if the condition

$$\boldsymbol{\kappa} = \mathbf{k} - \mathbf{k}' = \boldsymbol{\tau} \quad (23)$$

is fulfilled. This condition cannot possibly be satisfied below the Bragg-cutoff energy

$$\varepsilon_B = \tau_{\text{min}}^2 / (8m_n), \quad (24)$$

in which τ_{min} denotes the value of the shortest vector $\boldsymbol{\tau}$ with $F_N(\boldsymbol{\tau}) \neq 0$. In the case of hcp crystal with the following basic vectors of the inverse lattice

$$\begin{aligned} \boldsymbol{\tau}_1 &= c(1, 1/\sqrt{3}, 0), & \boldsymbol{\tau}_2 &= c(0, 2/\sqrt{3}, 0), \\ \boldsymbol{\tau}_3 &= c(0, 0, \sqrt{3}/8), \end{aligned} \quad (25)$$

where $c = 2\pi/a_{\text{hcp}}$, the Bragg-cutoff energy is determined by the vector $\boldsymbol{\tau}_{\text{min}} = [1, 0, 0]$. This corresponds to $\varepsilon_B \approx 2$ meV for sD₂ at low pressure.

When sD₂ has a random polycrystalline structure, the cross section (21), derived for a monocrystal sample, can be averaged over all orientations of the lattice. This leads to the polycrystalline cross section

$$\left(\frac{d\sigma}{d\Omega}\right)_{\text{coh}}^{\text{el}} = \frac{2\pi^2}{V_0} \frac{1}{k^2} \sum_{\tau} |F_N(\tau)|^2 \frac{1}{\tau} \delta\left(1 - \frac{\tau^2}{2k^2} - \cos\vartheta\right) \exp(-2W), \quad (26)$$

ϑ being the angle between vectors \mathbf{k} and \mathbf{k}' . If a mosaic sD₂ monocrystal is considered, Eq. (21) is numerically averaged over the Gaussian distribution

$$g(\alpha) = \frac{1}{\alpha_0 \sqrt{2\pi}} \exp\left(-\frac{\alpha^2}{2\alpha_0^2}\right), \quad (27)$$

of angular deviation α of the mosaic blocks from the mean direction. The standard deviation α_0 , which is usually called the mosaic spread, is here a free parameter.

The total differential cross section for neutron scattering in sD₂ is a sum of the incoherent cross sections (1) and (7), with \mathcal{S}_i given by Eq. (14), and the coherent Bragg cross section (21). For fixed initial energy ε and rotational state K , all possible rotational and vibrational transitions are included in this cross section. The total cross section σ_{tot} is thus given as

$$\sigma_{\text{tot}} = \int d\varepsilon' d\Omega \left[\sum_n \left(\frac{\partial^2 \sigma}{\partial \Omega \partial \varepsilon'} \right)_{0n} + \left(\frac{\partial^2 \sigma}{\partial \Omega \partial \varepsilon'} \right)_{\text{incoh}} \right] + \int d\Omega \left(\frac{d\sigma}{d\Omega} \right)_{\text{coh}}^{\text{el}}, \quad (28)$$

where the coherent fraction is calculated using Eq. (21) or Eq. (26), depending on the structure of a sample. If several rotational states are initially populated, the incoherent fraction of σ_{tot} is additionally averaged over a distribution of these states. At $\varepsilon \gg \varepsilon_B$, the coherent effects are negligible and therefore the total cross section is solely determined by the incoherent processes. At $\varepsilon \gg \omega_D$, effects of molecular binding in the lattice can be neglected and thus the cross section for sD₂ (per one molecule) corresponds to that for a free D₂ molecule.

III. RESULTS

Below, the calculated cross sections are compared with the experimental total cross sections for cold neutrons [1, 2], which were determined from neutron-beam attenuation in sD₂ samples. The purpose of the experiment was to study sD₂ as the UCN converter. The measurements were performed in almost pure ortho-D₂ ($98.7 \pm 0.2\%$), since a significant admixture of para-D₂ would drastically decrease the UCN lifetime [29], due to the neutron energy gain during the rotational relaxation $K = 1 \rightarrow K' = 0$ in D₂. Therefore, the present calculations have also been performed for pure ortho-D₂. In comparison with the experimental data it is assumed that the sD₂ target is small so that the neutron leaves the crystal after a single scattering and thus the kinematic diffraction theory is applicable. All available data are normalized to the value of 4.1 b at $\lambda = 6.5$ Å and $T = 8$ K [18], which is due to problems in accurate normalization of the measured cross sections.

The calculated total cross section for cold neutron scattering in a polycrystalline sD₂ at temperature $T = 8$ K and 15 K is shown in Fig 1. One can see that a very good agreement with experiment is reached for $\lambda \gtrsim 6.5$ Å, where there is no Bragg scattering and the total cross section is practically determined by the incoherent processes. Also, a good agreement is visible for $\lambda \gtrsim 2$ Å, where a contribution of the Bragg scattering to the total cross section is not dominant.

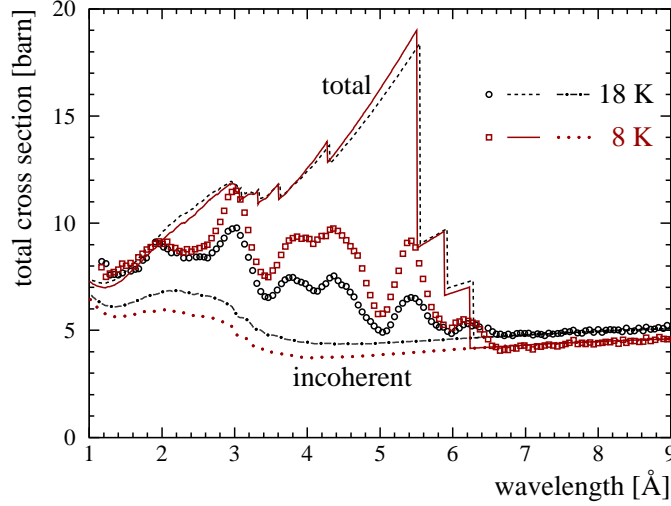


FIG. 1: Calculated (solid and dashed lines) and experimental (squares and circles, from Fig. 4 of Ref. [2]) total cross sections for cold neutron scattering in a polycrystalline ortho-D₂ at temperature $T = 8$ K and 18 K as functions of neutron wavelength. Also are shown the calculated incoherent contributions to the total cross sections (dotted and dot-dashed lines).

The incoherent cross section is greater at $T = 18$ K since the phonon processes are more probable at higher temperatures. On the other hand, the calculated Bragg cross section is greater at $T = 8$ K because the Debye-Waller factor is smaller at higher temperatures. Similar results were obtained in Ref. [17], with the use of $Z(\omega)$ derived from experiments.

Different contributions to the total incoherent cross section are shown in Fig. 2, for a solid ortho-D₂ at $T = 8$ K. The interval $\lambda \approx 4\text{--}7$ Å is dominated by the incoherent strictly-elastic scattering. The cross section of this process is described by the first term of expansion (14). The purely phonon processes are most significant in the vicinity of $\lambda = 2$ Å. The rotational-vibrational excitations begin to dominate the incoherent cross section above the first rotational threshold at $\lambda \approx 1$ Å, which corresponds to the excitation $K = 0 \rightarrow K' = 1$. Since in sD₂ this excitation may take place with simultaneous phonon annihilation, the respective cross section is visible up to $\lambda \approx 3$ Å.

The theoretical curves in Fig. 1 suggest that the experimental samples were not random sD₂ polycrystals. In the interval $\lambda \approx 2\text{--}6.5$ Å, the experimental data display several broad peaks with similar widths. The magnitudes of theoretical sharp peaks are mostly much larger and practically do not depend on temperature. Their locations do not fully coincide with the locations of observed peaks. In order to understand this problem, it is reasonable to consider neutron scattering in sD₂ monocrystal at various orientations. In comparison of theory with experiment, it is necessary to take into account the wavelength uncertainty $\Delta\lambda \approx 0.05$ Å [18]. This value is too small to explain the presence of broad Bragg peaks in a monocrystal sample. Therefore, a possible mosaic structure in the sD₂ monocrystal is considered, which can lead to a significant broadening for a sufficiently large value of the mosaic spread.

The calculated total cross section for cold neutron scattering from a 8-K sD₂ monocrystal oriented in the [2,0,1] direction is shown in Fig. 3. A mosaic structure of the monocrystal, with the spread $\alpha_0 = 3^\circ$, has been assumed. Also, the wavelength resolution is taken into account. The plotted experimental data [1, 2] for the three 8-K samples demonstrate that the specific structures of

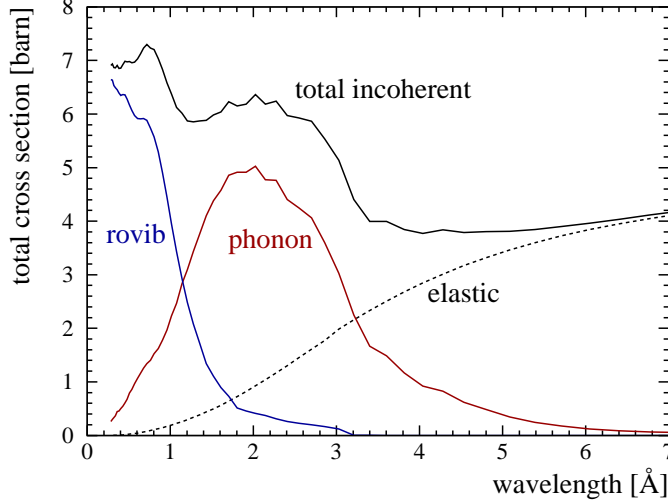


FIG. 2: Calculated contributions to the total incoherent cross section as functions of the neutron wavelength, for a solid ortho-D₂ at $T = 8$ K. The label “elastic” corresponds to the incoherent strictly-elastic scattering. A sum of the phonon creation and annihilation cross sections, with $\Delta E = 0$, is denoted by the label “phonon”. A sum of the rotational-vibrational transitions with possible simultaneous phonon processes is represented by the label “rovib”.

sD₂ were different, although freezing conditions were very similar. The two samples were frozen from liquid D₂ (labels “liquid 1” and “liquid 2”) and one sample was obtained by freezing D₂ gas (label “gas”). The presence of various patterns of Bragg scattering is obvious, if the considered samples were, at least in part, monocrystals grown in different orientations with respect to the incident neutron beam. Some peaks of the calculated cross section approximately correspond to the peaks observed in the “liquid 2” target. On the other hand, the calculated Bragg maximum at 4 Å is visible in the “liquid 1” case. The mosaic spread of about 3° is optimal — an increase or decrease by 1° leads to a worse agreement with the experiment. As one may expect, in the limit $\alpha_0 \rightarrow 180^\circ$ the theoretical cross section tends to the polycrystalline pattern, independently of a chosen crystal orientation.

The cross sections calculated for all the orientations $[h, k, l]$ with $h, k, l = 0, 1, \dots, 10$ do not accurately reveal the observed Bragg patterns of the three samples. This suggests that these samples could be composed of a certain number of large mosaic monocrystals. Visible cracks and optical opacity of the sD₂ targets [1, 7], which vary with temperature, support such a model. The total cross section in Fig. 4 has been obtained for the superposition of two crystal orientations: $[5, 0, 2]$ with the probability $\mathcal{P} = 0.45$ and $[5, 5, 2]$ with $\mathcal{P} = 0.55$. The theory quite well reveals the locations of Bragg peaks for the “liquid 2” sample. The differences between magnitudes of the calculated and experimental peaks do not exceed 30%. In the “liquid 1” case, which is presented in Fig. 5, an approximate description of the data has been achieved assuming the presence of three following monocrystal orientations in the sample: $[1, 0, 3]$, $[1, 1, 3]$, and $[2, 0, 1]$. Here they have the same probability $\mathcal{P} = 0.33$.

The peaks of the measured cross section for the “gas” sample are less pronounced than the peaks observed in the “liquid 1” and “liquid 2” targets. This can probably be ascribed to the lack of local correlations between D₂ molecules in gaseous deuterium. As a result, much more various orientations of sD₂ monocrystals are present in the “gas” sample, compared to the targets

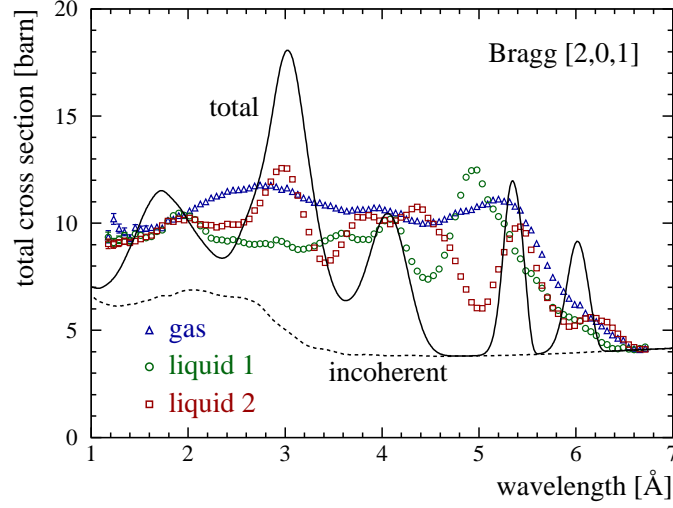


FIG. 3: Calculated total and incoherent cross section for cold neutron scattering from a 8-K ortho-D₂ monocrystal, oriented in the [2,0,1] direction, as a function of neutron wavelength. The mosaic spread $\alpha_0 = 3^\circ$ has been assumed. The experimental data for $T = 8$ K (from Fig. 5 of Ref. [2]) were determined using three different sD₂ targets, obtained by freezing D₂ gas (one sample) and D₂ liquid (two samples).

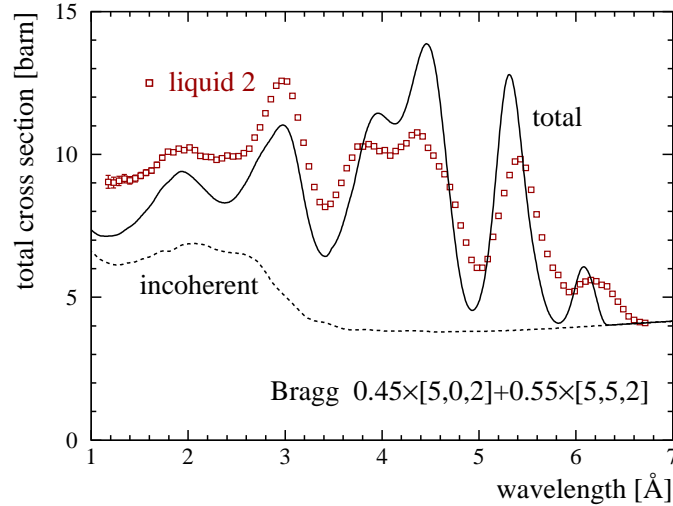


FIG. 4: Calculated total and incoherent cross section for cold neutron scattering from a 8-K ortho-D₂ target, which is composed of large hcp monocrystals oriented in the directions [5,0,2] (45%) and [5,5,2] (55%). The mosaic spread of 3° is assumed. The experimental 8-K data were measured using the sD₂ sample grown from liquid D₂ (“liquid 2”, Fig. 5 from Ref [2]).

grown from liquid deuterium. The theoretical cross section in Fig. 6 has been calculated assuming that the “gas” target is composed of the monocrystals that have orientations corresponding to the 69 shortest vectors of the inverse lattice (in the range $[0,0,1]$ – $[5,1,0]$). It is assumed that all the orientations have the same probability. The mosaic spread of 3° in every single monocrystal is also taken into account. One can see that the calculated total cross section roughly corresponds to the “gas” data. A better agreement with the experiment can be achieved by tedious adjusting the

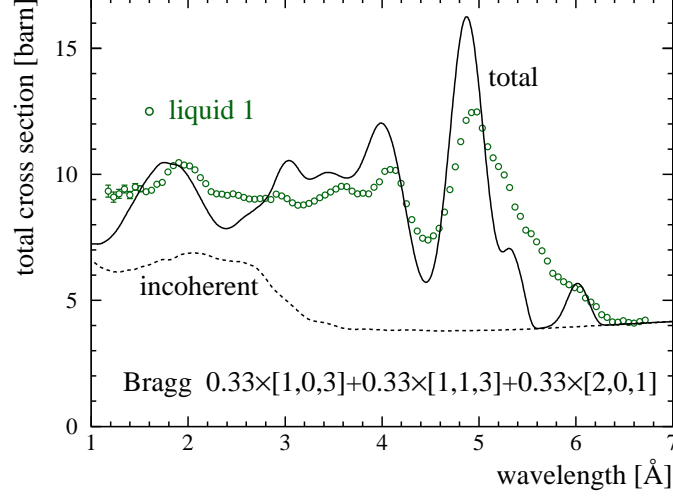


FIG. 5: Calculated total and incoherent cross section for cold neutron scattering from a 8-K ortho-D₂ target, which is composed of large hcp monocrystals oriented in the directions [1,0,3] (33%), [1,1,3] (33%), and [2,0,1] (33%). The mosaic spread of 3° is assumed. The experimental 8-K data were measured using the sD₂ sample grown from liquid D₂ (“liquid 1”, Fig. 5 from Ref [2]).

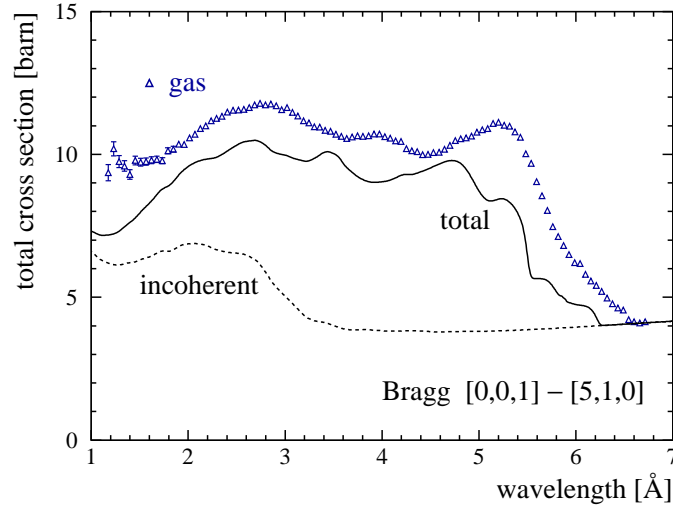


FIG. 6: Calculated total and incoherent cross section for cold neutron scattering from a 8-K ortho-D₂ target, which is composed of large hcp monocrystals oriented in all directions corresponding to the 69 shortest vectors of the inverse lattice (in the range [0,0,1]–[5,1,0]). The mosaic spread of 3° is assumed. The experimental 8-K data were measured using the sD₂ sample grown from a gaseous D₂ (“gas”, Fig. 5 from Ref [2]).

probabilities of various orientations, which are free parameters, and by using more monocrystal orientations, especially in the “liquid 1” and “liquid 2” cases. However, this is not a purpose of this work.

The experimental data shown in Fig. 1 were measured using the same “liquid 2” sample at $T = 8$ K and 18 K. The Bragg patterns for different temperatures, including 14 K and 17 K [1, 2],

are very similar. This means that the mosaic spread and orientations of macroscopic monocrystals do not significantly change, for a fixed sample. On the other hand, the magnitudes of observed Bragg peaks systematically decrease with rising temperature. This decrease is appreciable, especially when compared to the incoherent cross section which increases with rising temperature. The incoherent processes are well described by the theory. However, the calculated Bragg cross sections do not reveal strong temperature changes of the measured cross sections, both for the random-polycrystalline and monocrystal cases. A possible explanation is that multiple Bragg scattering took place in the sD₂ targets and, thus, the kinematic diffraction theory is not fully applicable to the considered experiment. In such cases, phenomena of primary and secondary extinction, which strongly depend on crystal structure and change the neutron-beam attenuation, should be taken into account (see e.g., Ref. [30] and references therein). In Fig. 7, the calculated

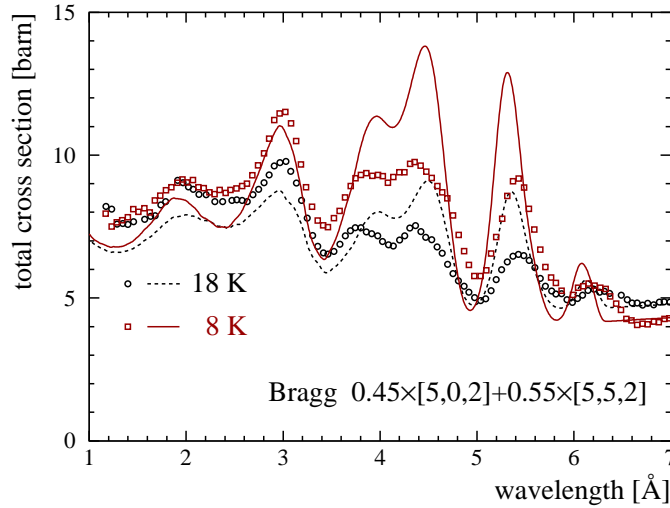


FIG. 7: The same as in Fig. 4 for $T = 8$ and 18 K of the “liquid 2” sample. A contribution from the Bragg scattering to the calculated total cross section at $T = 18$ K is scaled by the factor of 0.5.

total cross sections for the “liquid 2” sample at 8 K and 18 K are compared with the experimental cross sections. A qualitative agreement of theory and experiment is achieved here by scaling the 8-K Bragg cross section by a factor of 0.5.

IV. CONCLUSIONS

The calculated cross sections for cold neutron scattering in solid deuterium are in a reasonable agreement with the experimental data, if it is assumed that the sD₂ targets are composed of limited numbers of mosaic monocrystals with the mosaic spread of about 3°. In particular, this naturally explains the presence of different Bragg patterns in the sD₂ samples which are grown separately, although under very similar conditions. Such patterns are due to various orientations of the monocrystals, with respect to the impinging neutron beam. The magnitude of incoherent cross section and its variation with temperature is well described by the theory. On the other hand, the magnitude of measured coherent elastic cross section decreases strongly with rising temperature, which is not revealed by the theory. A possible explanation of this disagreement is that the kinematic diffusion theory is not valid for comparison of the theoretical cross sections with the experimental cross sections, which are determined using the neutron-beam attenuation method.

Although the presented cross sections have been calculated in the Bragg-scattering region, the conclusions regarding the sD₂ structure are of importance for scattering of ultracold neutrons and thus for developing high-intensity UCN sources. The phonon annihilation in ortho-D₂ is a crucial process which leads to UCN upscattering and, therefore, limits the effectiveness of sD₂ converters. Since the amplitude of neutron scattering from deuterium is mostly coherent, it is necessary to take into account a real target structure in the UCN-energy region. In estimations of the coherent phonon annihilation, the polycrystalline approach and neglecting crystal imperfections may lead to strong disagreement between theory and experiment. Figure 2 of Ref. [31], which shows strong changes of the UCN cross sections for different 5-K sD₂ samples, is an example of such disagreement.

Acknowledgments

I am indebted to M. Kasprzak for supporting the experimental data and explanations. K. Bodek and A. Kozela are acknowledged for discussions.

-
- [1] M. Kasprzak, Ultracold neutron converters, Ph.D. thesis, University of Vienna (2008).
 - [2] F. Atchison, B. Blau, K. Bodek, et al., Nucl. Instrum. Methods A 611 (2009) 252.
 - [3] R. Golub, K. Böning, Z. Phys. B 51 (1983) 95.
 - [4] A. Serebrov, V. Mityukhlyayev, A. Zakharov, et al., JETP Lett. 59 (1994) 757.
 - [5] A. Serebrov, V. Mityukhlyayev, A. Zakharov, et al., Nucl. Instrum. Methods A 440 (2000) 658.
 - [6] A. Sounders, J. M. Anaya, T. J. Bowles, et al., Phys. Lett. B 593 (2004) 55.
 - [7] K. Bodek, B. van den Brandt, T. Bryś, et al., Nucl. Instrum. Methods A 533 (2004) 491.
 - [8] F. Atchison, B. van den Brandt, T. Bryś, et al., Phys. Rev. C 71 (2005) 054601.
 - [9] A. Frei, Yu. Sobolev, I. Altarev, et al., Eur. Phys. J. A 34 (2007) 119.
 - [10] A. Serebrov, V. Varlamov, A. Kharitonov, et al., Phys. Lett. B 605 (2005) 72.
 - [11] C. A. Baker, D. D. Doyle, P. Geltenbort, et al., Phys. Rev. Lett. 97 (2006) 131801.
 - [12] R. Golub, D. Richardson, S. K. Lamoreaux, Ultra-Cold Neutrons, Adam Hilger, Bristol, 1991.
 - [13] G. Ban, K. Bodek, M. Daum, et al., Phys. Rev. Lett. 99 (2007) 161603.
 - [14] V. V. Nesvizhevsky, H. G. Börner, A. M. Gagarski, et al., Phys. Rev. D 67 (2003) 102002.
 - [15] I. F. Silvera, Rev. Mod. Phys. 52 (1980) 393.
 - [16] P. C. Souers, Hydrogen Properties for Fusion Energy, University of California Press, Berkeley, 1986.
 - [17] J. R. Granada, Europhys. Lett. 86 (2009) 66007.
 - [18] M. Kasprzak, private communication.
 - [19] W. H. Zachariasen, Theory of X-ray Diffraction in Crystals, Wiley, New York, 1945.
 - [20] E. Fermi, Ricerca Sci. 7 (1936) 13.
 - [21] L. Van Hove, Phys. Rev. 95 (1954) 249.
 - [22] S. W. Lovesey, Theory of Neutron Scattering from Condensed Matter, Clarendon Press, Oxford, 1984.
 - [23] A. Adamczak, Phys. Rev. A 74 (2006) 042718.
 - [24] A. Adamczak, Phys. Rev. A 76 (2007) 052512.
 - [25] M. Hamermesh, J. Schwinger, Phys. Rev. 69 (1946) 145.
 - [26] J. A. Young, J. U. Koppel, Phys. Rev. 135 (1964) A603.
 - [27] K. S. Singwi, A. Sjölander, Phys. Rev. 120 (1960) 1093.
 - [28] M. Nielsen, H. Bjerrum Møller, Phys. Rev. B 3 (1971) 4383.

- [29] C.-Y. Liu, A. R. Young, S. K. Lamoreaux, Phys. Rev. B 62 (2000) R3581.
- [30] V. F. Sears, Acta Cryst. A 33 (1977) 373.
- [31] F. Atchison, B. Blau, B. van den Brandt, et al., Phys. Rev. Lett. 95 (2005) 182502.